BBA - Bioenergetics xxx (xxxx) xxx–xxx

Contents lists available at ScienceDirect

BBA - Bioenergetics

journal homepage: www.elsevier.com/locate/bbabio

Network analysis of a proposed exit pathway for protons to the P-side of cytochrome c oxidase

Xiuhong Cai[a,b], Kamran Haider[a], Jianxun Lu[a], Slaven Radic[a], Chang Yun Son[c,1], Qiang Cui[c,2], M.R. Gunner[a,b,*]

[a] Department of Physics, City College of New York, 160 Convent Avenue, New York, NY 10031, USA
[b] Department of Physics, Graduate Center, City University of New York, 365 Fifth Avenue, New York, NY 10016, USA
[c] Department of Chemistry and Theoretical Chemistry Institute, University of Wisconsin-Madison, 1101 University Avenue, Madison, WI 53706, USA

ARTICLE INFO

Keywords:
Cytochrome c oxidase
Proton transfer
Grotthuss shuttling
Grand canonical Monte Carlo simulations

ABSTRACT

Cytochrome c Oxidase (CcO) reduces O_2, the terminal electron acceptor, to water in the aerobic, respiratory electron transport chain. The energy released by O_2 reductions is stored by removing eight protons from the high pH, N-side, of the membrane with four used for chemistry in the active site and four pumped to the low pH, P-side. The proton transfers must occur along controllable proton pathways that prevent energy dissipating movement towards the N-side. The CcO N-side has well established D- and K-channels to deliver protons to the protein interior. The P-side has a buried core of hydrogen-bonded protonatable residues designated the Proton Loading Site cluster (PLS cluster) and many protonatable residues on the P-side surface, providing no obvious unique exit. Hydrogen bond pathways were identified in Molecular Dynamics (MD) trajectories of *Rb. sphaeroides* CcO prepared in the P_R state with the heme a_3 propionate and Glu286 in different protonation states. Grand Canonical Monte Carlo sampling of water locations, polar proton positions and residue protonation states in trajectory snapshots identify a limited number of water mediated, proton paths from PLS cluster to the surface via a (P-exit) cluster of residues. Key P-exit residues include His93, Ser168, Thr100 and Asn96. The hydrogen bonds between PLS cluster and P-exit clusters are mediated by a water wire in a cavity centered near Thr100, whose hydration can be interrupted by a hydrophobic pair, Leu255B (near Cu_A) and Ile99. Connections between the D channel and PLS via Glu286 are controlled by a second, variably hydrated cavity.

Significance statement: Cytochrome C oxidase plays a crucial role in cellular respiration and energy generation. It reduces O_2 to water and uses the released free energy to move protons across mitochondrial and bacterial cell membranes adding to the essential electrochemical gradient. Energy storage requires that protons are taken up from the high pH, N-side and released to the low pH, P-side of the membrane. We identify a potential proton exit from a buried cluster of polar residues (the proton loading site) to the P-side of CcO via paths made up of waters and conserved residues. Two water cavities connect the proton exit pathway to the surface only when hydrated. Changing the degree of hydration may control otherwise energetically favorable proton backflow from the P-side.

1. Introduction

Cytochrome c oxidase (CcO) pumps protons from the N- (negative potential, high pH) to the P- (positive potential, low pH) side of a cell or mitochondrial membrane. The reaction is fueled by the reduction of oxygen (O_2) to water. In each reaction cycle, four electrons are transferred from cytochrome c^{2+} on the P-side to the binuclear center (BNC). The BNC is made up of heme a_3, Cu_B and a redox active tyrosine near the protein center. With each electron taken up by CcO, one proton is delivered to the BNC from the N-side and another proton is pumped

Abbreviations: CcO, Cytochrome c Oxidase; BNC, Binuclear Center; PLS, proton loading site; MD, molecular dynamics; PRA_{a3}, propionic acid A of heme a_3; PRD_{a3}, propionic acid D of heme a_3; PRA_a, propionic acid A of heme a; PRD_a, propionic acid D of heme a; P_R state heme a, Cu_A, and Cu_B oxidized with bound hydroxyl, ferryl heme a_3 and deprotonated Tyr 288; EP_{a3}^-, P_R state with protonated Glu286 and deprotonated propionic groups; EP_{a3}, P_R state with protonated Glu286 and protonated propionic acid A of heme a_3; E^-P_{a3}, P_R state with deprotonated Glu286 and protonated propionic acid A of heme a_3

* Corresponding author at: Department of Physics, City College of New York, 160 Convent Avenue, New York, NY 10031, USA.
E-mail address: mgunner@ccny.cuny.edu (M.R. Gunner).
[1] Current Address: Division of Chemistry and Chemical Engineering, California Institute of Technology, Pasadena, CA, 91125, USA.
[2] Current Address: Department of Chemistry & Department of Biomedical Engineering, Boston University, 590 Commonwealth Avenue, Boston, MA, 02215, USA.

https://doi.org/10.1016/j.bbabio.2018.05.010
Received 13 March 2018; Received in revised form 11 May 2018; Accepted 16 May 2018

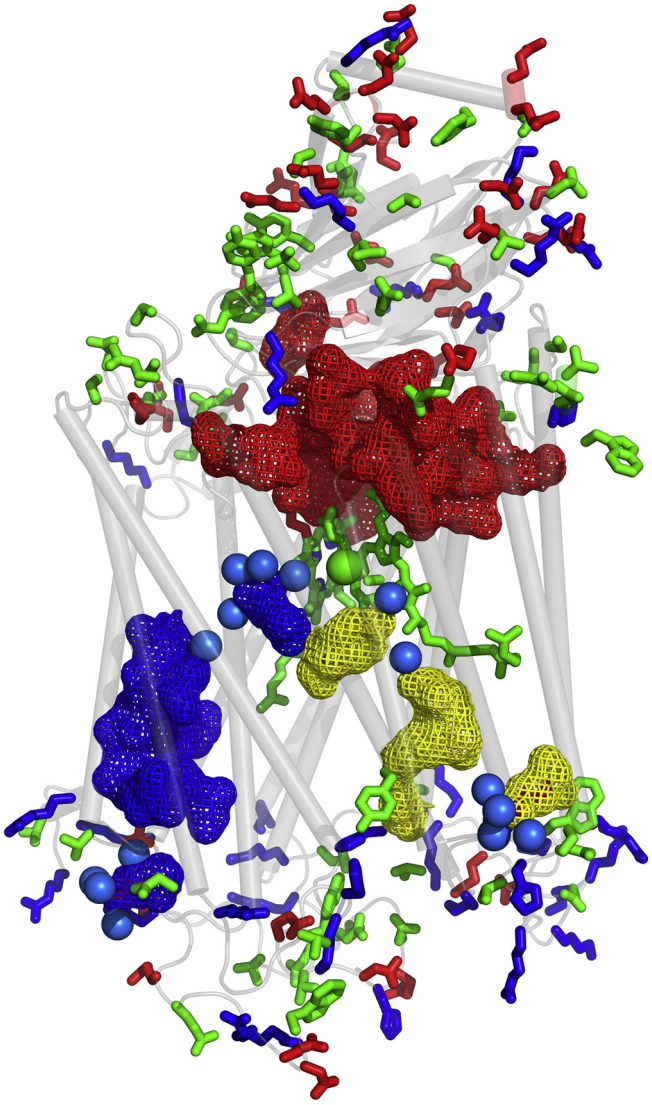

Fig. 1. Distribution of polar and protonatable residues in *Rb. sphaeroides* CcO (PDB ID: 1M56). Key residues have their side chains enclosed within mesh surfaces. Blue mesh: D channel; Yellow mesh: K channel; Red mesh: Buried, extended Proton Loading Site (PLS) cluster. Green sphere below PLS: CuB in the BNC; Blue spheres: waters around D and K channels. Green carbon sticks below PLS: heme a_3 in the BNC (right), and heme a (left). Sticks on the top and bottom: Side chains of all surface exposed ionizable and polar residues; in red: acid; blue: base; green: polar.

from N- to P-side. CcO thus increases the proton electrochemical gradient, providing energy for processes such as ATP synthesis [1]. The overall reaction is:

$$O_2 + 4Cytc_P^{2+} + 8H_N^+ \rightarrow 2H_2O + 4Cytc_P^{3+} + 4H_P^+$$

where the subscript indicates the P- or N-side. There are 4 distinct redox states of the BNC denoted R/P, F, O and E. R is the most reduced state of the BNC which is converted to P, the most oxidized BNC, when 4 electrons are donated to reduce O_2. The R to P transition requires no additional electrons. F, E and R are formed by sequential BNC reduction [2].

Protons travel via waters and polar side chains that are transiently protonated and deprotonated. The D- and K-channel proton uptake paths, through the generally non-polar N-side of A-type CcO, are easy to see in crystal structures (Fig. 1) [3,4]. Their importance has been established by mutating key residues [1]. The D-channel transports both chemical protons to be added to oxygen in the BNC and protons to be pumped to the P-side after being transiently bound in a Proton Loading Site (PLS). The K-channel provides chemical protons to the active site only during the O to E and E to R transitions [5]. The PLS is a residue or small group of residues whose proton affinity varies through the pumping cycle, so that one proton is bound from the D-channel via Glu286 and released to the P-side once in each of the four CcO redox states. The PLS has been proposed to be a propionic acid [2,6–10], a His ligand to Cu_B [10–14], a hydronium stabilized by fully ionized propionic acids [15] or distributed amongst several propionic acids [16] (which is assumed here). All of these groups are near each other and will be seen to be closely connected by water mediated hydrogen bonds.

In contrast to the N-side, there is no well-defined proton pathway on the P-side. Rather a large group of buried waters, polar and ionizable residues, interconnected by hydrogen bonds are found in a region that include all residues that have been proposed as the PLS. In addition, there are many P-side surface residues that could serve as proton outlets (Fig. 1). This complexity makes it hard to see how the thermodynamically favored proton loading from the P-side can be blocked. Earlier studies suggested potential P-side exit pathways in the related CcOs from different organisms. Proposed sites on exit paths in bovine CcO, include Lys171B/Asp173B, His24B/Asp25B, Asp51 and Asp300 [17] (bovine CcO numbering; B indicates subunit II[3]). Based on the electrostatic coupling between residues, the Lys171B/Asp173B pathway was considered to be the most promising candidate. In other studies, membrane potential-induced conformational changes were suggested to induce formation of a transient proton exit pathway [18]. An H channel leading from matrix to intermembrane space was proposed based on the bovine structure [19,20]. However, mutations of the analogous residues made in *Rb. sphaeroides* [21] and yeast [22] CcO do not support the H channel being required. The role of waters in the proton exit has also been investigated [23].

The work presented here carries out Grand Canonical Monte Carlo (MC) sampling on *Rb. sphaeroides* CcO crystal structures 1 M56 and 2GSM and snapshots from MD trajectories in the P_R state, varying the protonation state of Glu286 and the propionate A of heme a_3 (PRA_{a3}). The aim is to find hydrogen bonded pathways that are potential P-side proton exit pathways [24]. Network analysis of the hydrogen bonds shows highly interconnected clusters that contain functional residues such as Asp132 in the D-channel entry [25–29], the PLS propionic acids [8–10,13,16,30,31] and the critical Glu286 [7,32–38] that links the D-channel, the BNC and PLS. Network analysis newly identifies an extended, highly internally connected PLS cluster with ~16 residues all buried in the protein. In X-ray crystal structures the PLS cluster is disconnected from the P-surface or the D-channel. Hydrated cavities are found to open in the MD trajectories connecting the PLS cluster to the P-surface (P-exit cavity) and to the D-channel (Glu cavity). A novel, well-defined connection from the PLS propionic acids to the P-side surface via Thr100, Ser168, Asn96 and His93 is seen. The connection from the PLS depends on the hydration of the P-exit water cavity threading through these residues. The most common mechanism to close this path is when Ile99 and Leu255B come together, cutting the water chain in the middle. Similarly, a previously identified, dynamically hydrated cavity connects Glu286 and the PLS cluster when it is water filled (Glu286 cavity) [7,24]. The Glu286 cavity hydration depends mainly on the PRD_{a3} proton state in the MD trajectories [7,24], while the protonation state of Glu286 and redox state of heme *a* also make contributions.

[3] Lys171B/Asp173 (bovine) is equivalent to Lys227B/Asp229B (*Rb. Sphaeroides*); Asp25B (bovine) equivalent to Asp58B (*Rb. Sphaeroides*); His24B, Asp51, Asp300 in bovine has no corresponding residue in *Rb. Sphaeroides*.

2. Material and methods

2.1. MCCE calculations and hydrogen bond analysis

The calculations start with the crystal structure of *Rb. sphaeroides* (PDB code 1M56) [39], which was subjected to Molecular Dynamics in the P_R state with heme *a*, Cu_A, and Cu_B oxidized with bound hydroxyl, ferryl heme a_3 and deprotonated, anionic Tyr288. Trajectories are prepared in three substates that differ in the protonation state of the propionic acid of heme a_3 (PRA_{a3}) and of Glu286 (Table S1). The trajectories are designated by Glu (E) and propionic acid (P_{a3}) being neutral or negative. Thus, EP_{a3}^- has all four propionic acids deprotonated and Glu286 protonated. This is assumed to occur after heme *a* reduces the BNC prior to the proton translocation to the BNC [40]. The other two substates are generated from the equilibrated structure from the EP_{a3}^- trajectory after a 50 ns simulation. One has a deprotonated Glu286 and protonated PRA_{a3} representing proton transfer to the PLS (E^-P_{a3}) and the other has both the PRA_{a3} and Glu286 protonated (EP_{a3}) which models a system where the PLS retains its proton with Glu286 reprotonated. These substates were chosen based on earlier work showing they modify the proton affinity of the PLS, favoring proton release [16] and that they would change the hydration of a cavity near Glu286 [7]. The MD methods and parameters have been used previously [7,16] and are described more fully in the supplementary information. MCCE calculations and subsequent hydrogen bond network analysis are performed on 33 snapshots, with 11 extracted from each of the three MD trajectories, as well as on X-ray crystal structures 1 M56 and 2GSM.

The MCCE calculations use MC sampling to generate the Boltzmann distribution of hydrogen bond networks given backbone and side-chain carbon and buried water oxygen positions from the MD trajectory or crystal structures [41]. The methods and parameters used have been previously applied to CcO [7,16,42]. Thus, residue ionization states, polar proton positions, His tautomers and water occupancies are equilibrated given fixed side chain positions (referred to as isosteric sampling [41]). Surface waters with > 5% solvent accessibility in the input structure are removed and replaced with continuum solvent. All buried water oxygens are given 20–100 different proton positions and they undergo Grand Canonical MC sampling (see Table S2 for statistics of waters retained in GCMC analysis); the use of Grand Canonical sampling makes the results less dependent on the water occupancy in the MD snapshots. Hydrogen bond donors and acceptors are defined for each residue ionization state (Table S3). A hydrogen bond has a donor hydrogen-acceptor distance between 1.2 Å and 3.2 Å, and angle between donor D-H and acceptor > 90°.

MC sampling of each snapshot evaluates 24 to 42 million microstates. A water mediated connection is counted if positions that can form a hydrogen bond between two residues are chosen in > 0.1% of the microstates in a given snapshot. The analysis recognizes waters often connect residues or ligands. The default networks allow as many as 4 waters to bridge a connection. Fig. S1 shows the effect of changing the number of waters that connect residues. Connections in different snapshots are often made via different mobile waters. The connections made for individual snapshots in a trajectory are merged for the final analysis. Figs. S2 and S3 show the connections by the analysis of single snapshot or crystal structures. This initial analysis is quite permissive, as the connecting orientations of adjacent groups need not be found in the same microstate. The key paths between PLS and the P-surface are verified by identifying that there is a continuously hydrogen-bonded path between a defined beginning and ending residue in individual GCMC microstates. The networks are displayed using Cytoscape [43].

3. Results and discussion

3.1. Characterization of the CcO hydrogen bond network and P-exit cluster

The aim is to identify the hydrogen bond pathway(s) from the propionic acid Proton Loading Site (PLS) to the P-side surface. The CcO structure has 807 amino acid residues and 6 cofactors. Of these, 312 residues have polar or charged side-chains that can form hydrogen bonds. The CcO crystal structures identify the positions of C, N and O atoms, but drawing a hydrogen bond network requires defining the location of all polar protons and the protonation state of all resides. While the real protein crystal structure is in a Boltzmann distribution of protonation states and atomic positions, this information is lost in the reported coordinates. In contrast, MD trajectories save all proton positions in a single protonation state, at a small number of time points. MC sampling in MCCE is used to generate a Boltzmann ensemble of microstates, each with defined proton positions and protonation states given fixed heavy atom positions from an MD snapshot or crystal structure. Approximately 25×10^6 microstates are subjected to Metropolis sampling [44]. Thus, the addition of MC sampling enhances the information about thermally accessible hydrogen bond networks in the protein derived from a crystal structure or MD trajectory.

Two crystal structures and multiple snapshots from MD trajectories in three protonation states were examined to determine the hydrogen bond networks in *Rb. sphaeroides* CcO. Seventy-four core residues are found in strongly internally connected clusters (Table 1). Residues are often connected via waters. The default network described here allows groups to be connected by as many as 4 waters. The effect of changing the number of connecting waters on the network is discussed below. We will start by describing the network that is generated by combining the connections made in 11 snapshots of the most inter-connected MD trajectory, showing all found connections. Then we will see how connections are broken in a single experimental crystal structure or MD snapshot, with different numbers of bridging waters or in MD trajectories run with different protonation states of PRA_{a3} and Glu286. All the pictures of the two-dimensional networks maintain residues in the same positions to allow for visual comparison (Figs. 2B,C,D and S1, S2, S3, S4). Network placement highlights highly interconnected clusters, but only roughly mirror the residue positions in the three-dimensional structure (Fig. 2A). As will be seen CcO maintains well-defined clusters in all structures, but the connections between the clusters depend on the hydration of specific cavities that vary between structures.

Fig. 2B depicts the network derived from connections made in 11 snapshots from an MD trajectory run in the P_R state with Glu286 deprotonated and PRA_{a3} protonated, designated E^-P_{a3} (Table S1 defines

Table 1
Residues belonging to clusters in CcO hydrogen bond network.

Cluster	Residues
N-surface	D28, E548, H26, H549, K27, N25, N140, R19, S23, S544, T24, T550, W144, Y122
D-channel	D132, E286, N121, N139, N207, S142, S197, S200, S201, T211, Y33
K-channel	K362, S231, S299, T359, W366, Y288
BNC	Heme a_3 ($Fe(IV) = O^{2-}$), $Cu_B(II)$-OH^-
PLS	D407, D412, D229B, E254B, H411, PRA_{a3}, PRD_a, PRD_{a3}, Q276, R481, R482, S218B, T337, W172, W280, Y175
PLS'	N494, PRA_a, Q471, R52, S497, S498, Y414
P-exit	E182, H93, N96, N170B, R257, S156, S168, S186, T100, T187, W95, Y262B
P-exit'	D188, D485, E488, N91, N258, Q165
Cluster 1[a]	Q44B, K227B, Q251B, S253B, Y483, Y409, Q37B, Q477, T220B, T492, W493
Cluster 2[a]	D271, Q127B, R234B, T211B, Q345, Q126B, Q228B, R408, S48B, W239B

Residue name (single-letter code for amino acids) followed by *Rb. sphaeroides* CcO residue number. All residues are in subunit I unless marked with the 1-digit chain designator (B) if in subunit II. PRA_a and PRD_a are the propionic groups of heme *a*. PRA_{a3} and PRD_{a3} are the propionic groups of heme a_3. Surface residues (determined in the E^-P_{a3} MD trajectory) are underlined. Several ligands of Mg^{2+} (H411, D412 and E254B) are in the PLS cluster.

[a] Cluster 1 and Cluster 2 are connected to the PLS in a small number of snapshots. They are not discussed further or included in the network drawings.

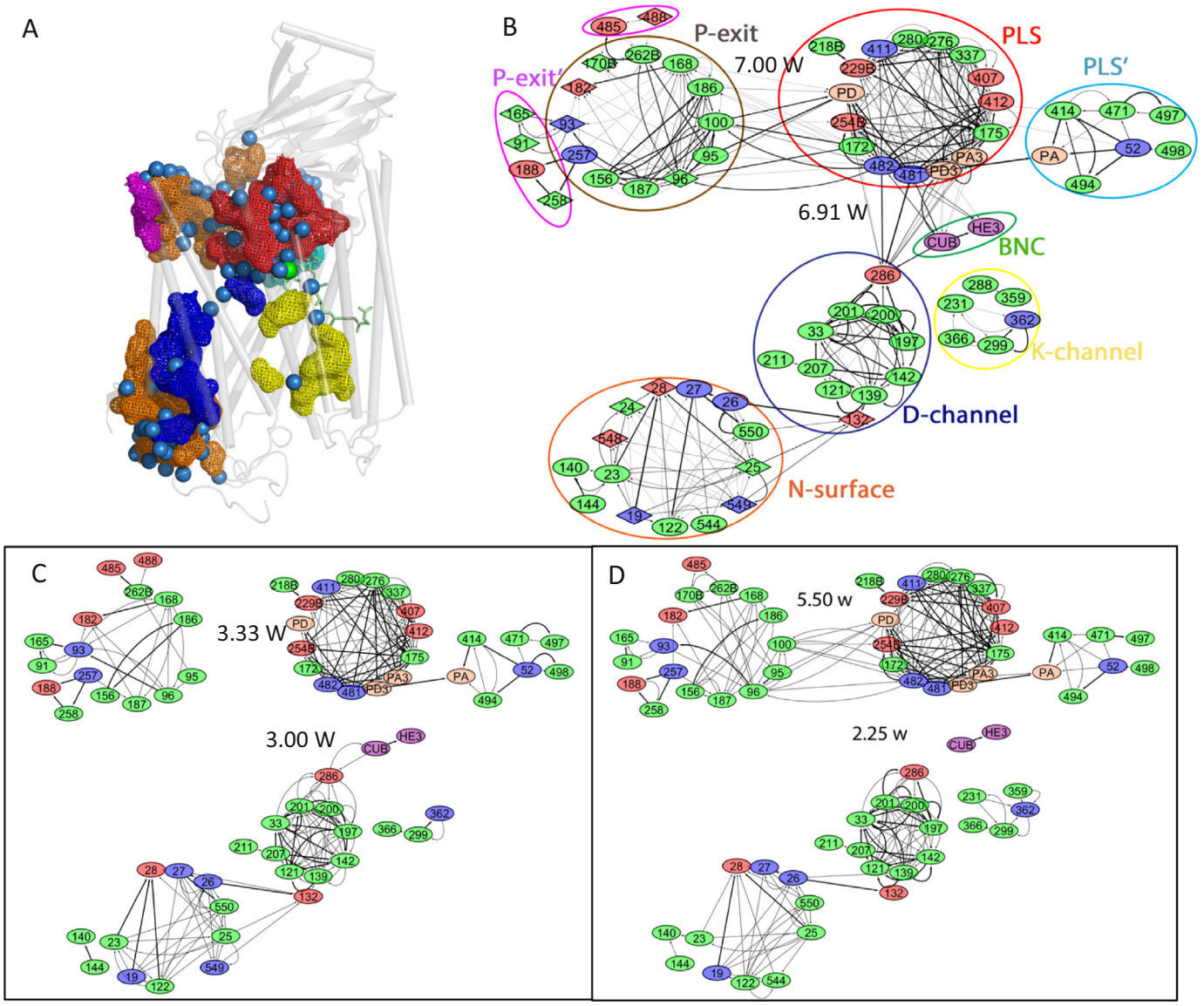

Fig. 2. Hydrogen bond networks in CcO. (A) *Rb. sphaeroides* CcO side chains in different clusters in surface mesh; orange: N-surface, blue: D-channel, yellow: K-channel, red: PLS, cyan: PLS', brown: P-exit, purple: P-exit'. Waters (blue) and Cu_B (green) are spheres, hemes are shown as sticks. (B) Hydrogen bond network based on MCCE analysis of E^-P_{a3} snapshots (Glu286 deprotonated and PRA_{a3} protonated), with well-hydrated Glu286 and P-exit cavities. Each line represents a direct side-chain hydrogen bond or one mediated by up to 4 waters (see Fig. S1 to see the dependence of the networks on the number of bridging waters). The nodes are colored based on the amino acid type; red: acid; blue: base; green: neutral polar; orange: propionic acids; purple: BNC; diamonds: surface residues. Clusters are surrounded by ellipses of the same colors as in A. For clarity only the residue number is given for each node (Table 1 lists residue names for each node. PA, PD, PA3, PD3 represents PRA_a, PRD_a, PRA_{a3}, PRD_{a3} respectively). All network figures place all nodes in the same location. The numbers between the clusters are the average hydration level of Glu286 cavity (between Glu286 and PLS clusters) and the P-exit cavity (between PLS and P-exit clusters). (C) Hydrogen bond network at 0 ns, 3 ns, 7 ns in the EP_{a3}^- trajectory with relatively low hydration of Glu286 and P-exit cavities, which breaks the inter-cluster connections between PLS & P-exit and Glu286 & PLS. (D) Hydrogen bond network at 20 ns, 32 ns, 38 ns, 50 ns in EP_{a3}^- trajectory with a relatively low hydration of Glu286 cavity, and well-hydrated P-exit cavity. This breaks the inter-cluster connections between PLS and Glu286, while PLS still connects to the P-exit. Substate nomenclature, E represents Glu286, and P_{a3} the PRA_{a3}. Therefore, EP_{a3}^- is P_R state with protonated Glu286 and all deprotonated propionic groups; EP_{a3} has Glu286 and PRA_{a3} protonated; while E^-P_{a3} has deprotonated Glu286 and protonated PRA_{a3}.

redox and protonation states fixed in each trajectory). The D-channel, K-channel, BNC and PLS cluster form self-connected regions (Table 1). Glu286 is the well-established hub connecting the D-channel, BNC and PLS. The PLS propionic acids are part of a highly interconnected PLS cluster. Glu101B, which was proposed to be the K-channel entrance [45,46], is not connected to the K-channel cluster in any trajectory. In addition to Asp132, only the N-surface, P-exit and associated P-exit' clusters have surface exposed residues. Two extra P-side clusters (Cluster 1 and Cluster 2), adjacent to the PLS cluster are found to be connected in only a few snapshots. Other residues form much smaller, isolated networks that do not connect to the BNC, PLS cluster or D or K channel clusters in any MD or PDB structures.

3.1.1. *N-side networks*

While the identity of the exit to the P-side represents the key finding here, we will first briefly describe the N-side connections, which are in agreement with previous studies [7,25–29,32–38,47,48]. The D-channel is an internally well-connected cluster with a unique entrance at Asp132 and exit at Glu286. The network analysis identifies a novel N-surface cluster that connects the D-channel via Asp132 to a set of

surface-exposed residues. The N-surface cluster could serve as an antenna for proton capture from the compartment with low proton chemical potential, a feature of CcO that was suggested by earlier measurements of the pH dependence of N-side proton uptake [49]. Six of the fourteen N-surface cluster residues are surface exposed including the ionizable residues His549, Asp28 and Glu548. The K-channel cluster, is isolated, with no connection to the BNC or the surface [4,50]. This may be a result of its only transferring protons to the BNC in the O to E to R steps, so it may not be connected in the P_R state studied here [5].

3.1.2. P-side networks

The network on the P-side of the protein shows a highly interconnected group of 16 residues identified as the Proton Loading Site (PLS) cluster. The PLS propionic acids are postulated to transiently hold protons prior to their expulsion to the P-side [8–10,13,16,30,31]. Previous studies [16] have shown that the proton affinity of the propionic acids in this complex environment are poised so they will change protonation state, loading a proton and releasing one as the electrons are transferred to heme *a* and on to heme a_3 and protons move to the BNC. The PLS cluster has 7 acidic residues and only 3 basic ones. These include His411, Asp412 and Glu254B that are Mg^{2+} ligands as well as Glu254B that is one of the ligands to Cu_A.

Allowing hops through a maximum of 4 waters, each PLS cluster residue is connected to at least 6 other cluster members. This suggests that a proton bound to any residue in the PLS cluster can easily find the sites with the highest proton affinity. Previous MCCE studies showed that the four propionic acids function as a distributed proton loading site [16], while other residues rarely change their equilibrium protonation as the PLS loads and releases protons. However, the PLS cluster residues play a role in setting the proton affinity of the propionic acids and permit the proton to move though the highly extended, buried cluster. A weakly connected PLS' cluster is also identified. Neither PLS nor the PLS' clusters contain any surface exposed residues.

3.1.3. Pathway from the PLS to the P-surface

The P-side surface of CcO contains ~46 solvent exposed polar residues. It has not been established how the PLS connects to the surface [21,22]. The network drawn in Fig. 2B is very permissive in identifying connections. Here two residues are connected if they form direct or water mediated hydrogen bonds, with four or fewer intervening water molecules, in at least 0.1% of the equilibrated microstates. What is striking is how few surface residues (Diamond shaped nodes in Fig. 2B) are connected to the internal clusters on the P-side (or the N-side) of CcO. Thus, despite the highly interconnected PLS cluster in the center of the P-side, which extends over ~20 Å, there are few connections to the surface. The identified path in the network from PLS to the surface is via the P-exit cluster, containing 12 residues (Table 1). The P-exit cluster is connected to the P-exit' cluster with 6 residues. The P-exit' cluster spans three water connected locations, each with a pair of residues. The P-exit and P-exit' clusters each have 4 surface exposed residues.

The well-connected hydrogen bond network found in the E^-P_{a3} trajectory is analyzed to find the sites with the largest number of shortest paths between all possible pairs of residues (nodes) (Fig. S4). The pivotal groups in the PLS cluster are the PLS propionic acids PRD_a, PRA_{a3} and PRD_{a3} and Glu254B. The P-exit cluster links to the PLS cluster via Ser168, Ser186, Thr100, Asn96 and Trp95. The key surface-exposed residues are His93, Glu182 and Glu488 in the P-exit or P-exit' clusters.

A given snapshot can be analyzed in different ways. The default network analysis defines side chains as being connected if a hydrogen-bonded path between them can be found via four or fewer waters. To understand the importance of waters, the hydrogen bond network is calculated with different cutoffs for the maximum number of waters bridging residues (Fig. S1). With no intervening waters, few residues are connected, highlighting the importance of waters. However, there is little difference between networks with 3, 4 or 5 connecting waters, and 4 is the default here.

The network found for a series of individual E^-P_{a3} snapshots (Fig. S2) shows the persistence of hydrogen bonds through the MD trajectory. There is some variation in connectivity within N-surface and P-exit clusters in individual snapshot. However, the clusters and their interconnections remain relatively intact, with connection from the PLS to the P-exit cluster retained in all snapshots from this trajectory.

3.2. Hydration controls connectivity in P-side networks

In the MCCE analysis of the E^-P_{a3} trajectory, all clusters, except the K-channel, are interconnected. Analysis of crystal structures and different MD trajectories identify cavities whose changing hydration modulates the inter-cluster connections in a manner that can contribute to the control of CcO proton transfers. The hydrogen bond networks were determined in two X-ray structures of CcO (PDB ID: 1M56 and 2GSM), retaining the experimental, buried water positions. Each crystal structure (Fig. S3) is better compared with a single MD snapshot (Fig. S2) than with the network formed by merging the connections found from multiple snapshots (Fig. 2B). The X-ray structure networks show all internally connected clusters seen in Fig. 2B. The P-exit and N-surface clusters revealed in the analysis of MD snapshots can be seen in hindsight in the crystal structure. However, the water-mediated inter-cluster connections between D-channel and the PLS via Glu286 and from the PLS cluster to the P-exit are lost.

Two additional P_R MD trajectories were analyzed. One fixed Glu286 protonated and all propionic acids ionized (EP_{a3}^-) and another kept both acids neutral (EP_{a3}). In each case 11 snapshots from a given trajectory were subjected to MCCE network analysis and the results merged. The connections within clusters remain in all snapshots in all trajectories; however, the inter-cluster connections vary (Table 2, Fig. 2B, C, D). Thus, connections from the D-channel to the PLS (Fig. 2C, D) or from the PLS to the P-exit (Fig. 2C) are broken. Two cavities, designated the Glu286 cavity and P-exit cavity, are found to control the inter-cluster connectivity to and from the PLS in the X-ray crystal structures and the MD trajectories. The P-exit cavity hydration is assigned as the number of waters within 3.5 Å of side-chain polar atoms of Thr100, Trp95 or Asn96 (Table S4). The Glu286 cavity hydration is assigned by the number of waters within 4.5 Å of the terminal oxygens of the Glu. The number of waters in these cavities and the cluster connectivity is summarized in Tables 2 and S4.

In the crystal structures the Glu286 and P-exit cavities are dry and the clusters unconnected. In the MD trajectories the cavity hydration fluctuations depend on the assigned propionic acid and Glu286 protonation state. After 50 ns in the EP_{a3}^- substate with all four propionic acids ionized, only two of the five water molecules initially added to the Glu286 cavity region are retained and inter-cluster connections are broken. However, when initiated with this dry Glu286 cavity, protonation of PRA_{a3} in the E^-P_{a3} substate shows a rapid increase of the hydration level in both the Glu286 cavity (as also seen in previous studies when PRD_{a3} was protonated [7]) and P-exit cavity as detailed here. In contrast, the EP_{a3} state retains a dry Glu286 cavity (see Table S4). Overall, the E^-P_{a3} trajectory is characterized by both cavities being well hydrated, EP_{a3} is significantly drier, while EP_{a3}^- fluctuates between dry and partially hydrated cavities. The wet to dry transition can occur over multiple tens of nanoseconds.

The Glu286 cavity has been described previously [7,51,52]. Hydration of this cavity has been shown to substantially lower the pK_a of Glu286, stabilizing proton loss and the E^-P_{a3} state[7]. MD simulations and free energy calculations [53] suggested that the Glu286 cavity opening is largely controlled by PLS propionic acid protonation, which perturbs the conformation of a nearby loop that contains Trp172 and thus the volume of the cavity; a deprotonated Glu286 further facilitates and stabilizes the hydration level increase in the cavity, while the cavity

Table 2
The Glu286 and P-exit cavity hydration and cluster connectivity summarized for different groupings of MD snapshots.

	E286[a]	P-exit[b]	E-orien[c]	PLS → PE[d]	E → PLS	D → E	E → BNC	BNC →PLS
$E^{-}P_{a3}$	6.91 ± 1.22	7.00 ± 1.10	10.0 ± 0.7	100%	100%	100%	73%	82%
EP_{a3}^{-}	2.82 ± 1.32	5.00 ± 1.55	10.3 ± 0.8	64%	0%	91%	18%	0%
EP_{a3}^{-} Wet	2.86 ± 1.35	5.71 ± 1.38	10.1 ± 0.7	100%	0%	100%	14%	0%
EP_{a3}^{-} Dry	2.75 ± 1.50	3.75 ± 0.96	10.7 ± 0.8	0%	0%	75%	25%	0%
EP_{a3}	1.45 ± 0.69	6.36 ± 1.12	11.7 ± 0.8	100%	0%	91%	0%	73%
1 M56	1	2	10.3	0%	0%	100%	0%	0%
2GSM	1	2	10.2	0%	0%	100%	0%	0%

EP_{a3}^{-} Dry snapshots have unconnected PLS and P-exit clusters, while in EP_{a3}^{-} Wet they are connected. The correlation between PLS → PE and E → PLS in individual snapshots: 33% both connected; 12% both disconnected: 54% PLS → PE but not E → PLS. There are no snapshots with E → PLS connected but PLS → PE unconnected.

[a] The number of waters within 4.5 Å of either terminal oxygen of Glu286.

[b] The number of waters within 3.5 Å of the side-chain polar atoms of Thr100, Asn95 or Trp94.

[c] The Glu286 orientation is defined by the distance in Å between Glu286 CD and heme a_3 CAD atoms. A distance of ≤10 Å indicates the Glu286 is pointing up towards the PLS, while with a distance > 11 Å it points down into the D channel.

[d] PLS → PE, E → PLS, D → E, E → BNC, BNC → PLS represent the percentage of the snapshots where inter-cluster connections between PLS and P-exit, Glu286 and PLS, D-channel and Glu286, Glu286 and BNC, BNC and PLS were found. The water occupancy and connectivity of each individual snapshot is found in Table S4. The residues in each cluster are listed in Table 1.

expansion and wetting transition occurs substantially more slowly when Glu286 is protonated [53]. As all Propionic acids are in the PLS (or PLS') clusters, a loaded proton can equilibrate amongst the different acids [16]. Thus, as the cavity hydration and resultant cluster connectivity may be triggered by the loading of the PLS, it need not be strongly dependent on which of these acids is protonated. We see here when at least 6 waters are present in the Glu286 cavity, the PLS and Glu286 are always connected. No snapshots with 4 or fewer waters within 4.5 Å of Glu286 show connections, while 5 waters may or may not mediate the connection.

The newly identified P-exit cavity connects the PLS and P-exit clusters. The P-exit cavity is bounded by Trp172, Arg482, Trp95, Asn96 and Thr100 (Fig. 3). The P-exit cavity is linear in contrast to the more spherical Glu286 cavity. With 6 waters in this cavity, the PLS cluster is connected to the P-exit cluster and with 3 or fewer it is not. With intermediate number of water molecules, the pathway need not be complete. The connection between Thr100 and PRD_a requires at least two waters.

The P-exit cavity is connected to a nearby loop, consisting of residues Gly167, Ser168, Gly169, Ile170, Gly171, Trp172 and Val173, including the highly conserved GxGxGWxxYxPL motif (Table S5). Elements of this loop had been previously found to determine the hydration of the Glu286 cavity [7]. Trp172 in the loop interacts directly with PRD_{a3}. On the top and bottom of the P-exit cavity, there is a hydrophobic pair, Leu255B and Ile99 (Fig. 3B, D). The pair moves apart when the P-exit cavity is wet, and they are closer when the P-exit cavity is dry. Leu255B is near Cu_A, whose one-electron reduction is coupled with one-proton pumping in CcO [54]. In the HSSP database [55], residue 255B is 76% Ile, and 23% Leu, with weight 0.76, while residue 99 is 63% Val, 22% Phe, and 7% Ile, with weight 0.47. Thus, they are almost always occupied by hydrophobic amino acids. This cavity is dry in the crystal structures and can be variably hydrated in a single trajectory. Thus, in contrast to our better understanding of how the propionic acids and Glu286 protonation states trigger and stabilize changes in the Glu cavity hydration, we do not know the specific set of conditions that will reproducibly change the P-exit cavity hydration.

Proton uptake to the PLS from the P-side must be controlled so that protons move uphill from N- to P-side. There will be no proton transfer if there is no pathway, thus changing cavity hydration is one method to block translocation. However, when connected paths are found the rates of competing proton transfers to N- or P-side of the membrane and to the PLS or BNC depend on multiple factors. These include: the metastable proton affinity of the PLS, Glu286 and BNC, which change through the reaction cycle [16]; the stability of pathways that are well oriented for proton transfer [56]; the energy of injecting a proton into the pathway [17,24,51] as well as the transmembrane electrochemical potential and ΔpH, which determines the overall back pressure on proton pumping [57,58]. The merged network generated from the trajectory with Glu286 and PRA_{a3} protonated shows interconnections between N-surface, D-channel, PLS and P-exit clusters (Fig. 2, Table S6). Many individual snapshots also show persistent connections between P- and N-side clusters (Fig. S2, Table S4). Thus, other factors would be needed to disrupt proton transfers in the wrong direction. The energetics of proton transfer that can reduce transfer in a connected path is outside of the scope of this paper.

3.3. Comparison with earlier studies

3.3.1. Residue conservation

The network analysis of *Rb. sphaeroides* CcO identifies Thr100, Ser168, Asn96, Glu182, Asp485 and Tyr262B as important residues for proton transfer to the P-side surface. An alignment of CcO sequences in the HSSP database [55] shows that Thr100, Asn96, Arg257 are highly conserved with a weight > 0.8. In contrast, His93 is often changed to the polar Gln while Glu182 is often found to be a non-polar Ile or Leu. These residues may play a role only in *Rb. sphaeroides* and closely related CcOs, or waters in the P-exit cavities may relax in the requirement for specific residues. Thus, the residues that directly connect PLS and the P-exit cluster are relatively conserved, whereas the surface exposed residues of P-exit cluster are more variable.

3.3.2. Suggested pathways

The residues on the proton transfer pathway proposed here were compared with those suggested in earlier studies. The network seen here (Table 1) does not include the N-side amino acids proposed to be part of the H-channel [18,19,21,22]. However, the auxiliary PLS' contains residues Gln471, Tyr414 and Arg52, Asn494, Ser497 which are part of the P-side of the proposed H channel.[4] In addition, the P-exit and P-exit' cluster contains Asn96, Trp95, His93, Asn91, equivalent to Gly49 to Asn55 in bovine CcO H channel [18]. The key H-channel residues are Tyr54 and Asp51 (bovine numbering). However, the Tyr is replaced with Trp95 (*Rb. sphaeroides*), while there is a gap in *Rb. sphaeroides* CcO in the region of Asp51.

[4] H channel sequence alignment: His413, Thr424, Ser461, Ser382, Ser454, Gln428, Arg38, Asn451, Tyr443, Tyr371, Try54, Asp51 (bovine) is equivalent to His456, Thr467, Ser504, Ser425, Ser497, Gln471, Arg52, Asn494, Try486, Tyr414, Trp95 (*Rb. Sphaeroides*). Asp51 has no *Rb. Sphaeroides* equivalent.

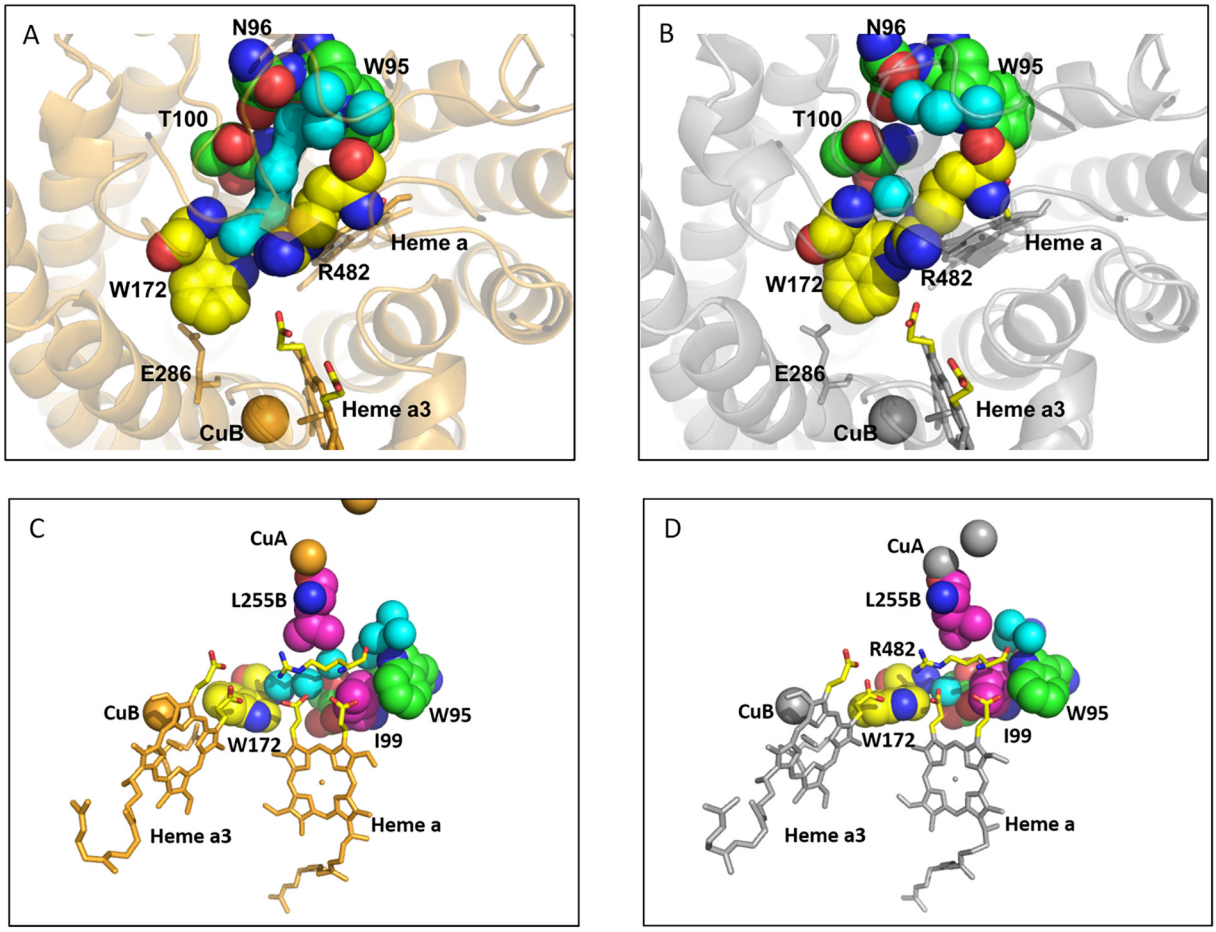

Fig. 3. P-exit cavity. Protein backbone is shown. Yellow carbon spheres used for W172 and R482 are in the PLS cluster, while T100, W95 and N96 in the P-exit cluster have green carbons. Water molecules are cyan spheres. (A, C) EP_{a2}^{-} snapshot with wet P-exit cavity. P-exit water wire is enclosed by cyan surface. The distance between L255B atom CG and I99 atom CB is 8.9 Å. (B, D) EP_{a3}^{-} snapshot with dry P-exit cavity. The distance between L255B atom CG and I99 atom CB is 7.2 Å. In A, B L258B and I99 are above and below the water wire. In C, D the view is rotated. The two hydrophobic groups have their carbons colored magenta.

Crystal structures of the bovine protein also show the segment Gly49 to Asn55 moves towards the cytosolic surface by about 4.5 Å near the carboxylate group of Asp51 on reduction of the fully oxidized enzyme [18]. These movements occur in the region near the P-exit pathway.

Studies of H/D exchange coupled to mass spectrometry identified segments of *Rb. sphaeroides* CcO where the exchange rates are altered in the E286H mutant, which turns over slowly without pumping [59]. Five residues in the PLS cluster (Gln276, Thr337, Trp172, Trp280, Tyr175), two in the P-exit cluster (Arg257, Ser168) and two in the P-exit' cluster (Asn258, Gln165) are in regions whose solvent exposure or protein dynamics are modified. Residues in other clusters did not show altered H/D exchange. There are other regions of the protein whose side chains exchange rates vary that are not found in the network investigated here.

Earlier calculations evaluated possible proton exit pathways in a bovine x-ray crystal structure by finding the amino acids in the region on the P-side that are coupled electrostatically to the His ligand to Cu_B that was assumed to be the PLS [11–14]. Residues that were found to change proton affinity when CcO moves between different redox states were proposed to provide a low energy proton transfer pathway [12]. The calculations thus identified sites for proton transfers in a manner that focused on electrostatic energy connections rather than hydrogen bond connections. Possible water pathways were also traced in bovine [23] and *Rb. sphaeroides* [53] CcO MD trajectories. The pathway in bovine CcO runs through the PLS cluster but not in the direction of the P-exit cluster. The analysis of the bovine trajectories considered transient hydrogen bond connections in snapshots, again suggesting pathways via His204B/Lys171B, which are not in the network found here.

The pathway to the P-surface found here is different from the ones identified earlier [17], which involved residues in the Mg^{2+} cluster and the Lys171B/Asp173B (bovine numbering; Lys227B/Asp229B here) pairs. In our analysis, Asp229B is one of the PLS cluster residues and Lys227B in the rarely connected Cluster 1. A proposed exit pathway for the product water runs near this Lys227B/Asp229B pathway [60]. The pathway addressed here runs in the same direction as one of the two water exchange pathways, which passes near His93/Glu182 [53]. While water and protons can use the same paths, our study highlights a separate path for the exit of protons.

3.3.3. *P-side mutational analysis*

While mutations of key N-side residues such as Asp132, Lys362 and Glu286 reduce activity in a clear-cut way, mutations on the P-side have often provide inconclusive results [48,59,61–66]. One reason may arise from the different styles of connections on P- and N-sides. The N-side D-channel has a unique entry (Asp132) and exit (Glu286) connected by a linear array of waters and polar residues, with no other ionizable groups. In contrast, the PLS on the P-side is part of the PLS cluster, a buried, highly interconnected region with 6 polar residues and 7 acids and 3 bases. The network analysis shows water mediated connections from Glu286 to multiple residues in the PLS cluster. In addition, while the P-exit is a highly localized region on the P-side surface, there are several discrete paths from the PLS to the surface that may contribute, making it hard to block transfer with a single mutation. A P-side that

can support some backward proton transfer allows non-energy conserving reactions with O_2 as the terminal acceptor at high proton motive force when protons may need to enter from the P-side to dissipate energy. Situations where CcO cannot accept electrons lead to ROS build-up from reduced complex I and III [57].

The extensive, interconnected PLS cluster may also contribute to unanticipated effects of mutating P-side residues. The ability of the PLS to bind and release protons relies on its changing proton affinity as well as its connections to the surface [16]. Thus, to bind and release one proton, the cluster must have an effective pK_a above 9 in the loading state and below 5 in the release state (assuming the pH is 7 and probability that a proton will be bound and released is 99%). The proton affinity is controlled by the redox states of Cu_A, heme *a* and the BNC, as well as the position and charge of the web of nearby polar and charged residues. Thus, mutations in the PLS such as of Arg482, Arg481 have had variable effects [65–67]. Additionally, residues such as His93 and Thr100, which are important nodes on the P-exit pathway, appear to modify the electrochemistry of Cu_A and heme *a*, making it difficult to isolate their role in proton transfer [67].

Support for the proposed P-exit network can be obtained from negative results, where mutation of residues that are not in our proposed networks in fact have little or no effect on CcO function. These include Ser504, Thr467, His456, Glu450, and Ser425 on the proposed H-pathway. These are mainly near but unconnected from the ancillary PLS' cluster, and were found to have little effect on proton pumping [18,21]. Mutations of the dead-end PLS' such as Q471A and Y414F, which do not change the charge, also do not change CcO function [21]. In contrast, R52A in the PLS' cluster does not support activity, which may be due to changes in PLS proton affinity rather than pathway connectivity. Thus, the network analysis while indicating a preferred pathway may also provide a rationale for the lack of difinitive results found for different P-side mutations in CcO.

4. Conclusions

While D and K channels are clearly delineated on the N-side of CcO, the cytochrome *c* oxidase structures do not identify a simple pathway for proton exit to the P-side. The hydrogen bond network analysis of CcO reveals an extended, but fully buried set of residues that from a PLS cluster. A small number of pathways leads from the PLS cluster to a cluster of residues on the P-side surface via the P-exit cavity. Glu286 is also seen as a hub connecting the D-channel, the PLS and the BNC. A variably hydrated water cavity near Glu286 allows a mechanism to modulate the connections between BNC and PLS.

The thermodynamically uphill transfer of protons from N- to P-exit requires a controlled exit pathway to avoid excessive thermodynamically favorable proton back-flow. Variable hydration of the PLS cavity near Thr100 can make or break the connection between the PLS and the P-side surface. When the Glu and PLS cavities are dehydrated the PLS is fully insulated from the surface of the protein. However, the changes in redox state or residue protonation that can reliably trigger connectivity changes in the exit pathway, are still unknown.

Transparency document

The Transparency document associated with this article can be found, in online version.

Acknowledgements

We would like to thank Xuyu Zhu for modifications of MCCE and Shelagh Ferguson-Miller for very helpful discussions. Research funded by grant number MCB-1519640 from the National Science Foundation. M.R.G. also acknowledges infrastructure support from the National Institute on Minority Health and Health Disparities (Grant 8G12MD007603) from the National Institutes of Health. Q.C. acknowledges National Science Foundation for the grant number NSF-CHE-1664906. Computational resources from the Extreme Science and Engineering Discovery Environment (XSEDE), which is supported by NSF grant number OCI-1053575, are greatly appreciated.

Appendix A. Supplementary data

Supplementary data to this article can be found online at https://doi.org/10.1016/j.bbabio.2018.05.010.

References

[1] M. Wikström, V. Sharma, V.R.I. Kaila, J.P. Hosler, G. Hummer, New perspectives on proton pumping in cellular respiration, Chem. Rev. 115 (2015) 2196–2221, http://dx.doi.org/10.1021/cr500448t.
[2] V.R.I. Kaila, M.I. Verkhovsky, M. Wikström, Proton-coupled electron transfer in cytochrome oxidase, Chem. Rev. 110 (2010) 7062–7081, http://dx.doi.org/10.1021/cr1002003.
[3] M.R.A. Blomberg, P.E.M. Siegbahn, Proton pumping in cytochrome c oxidase: energetic requirements and the role of two proton channels, Biochim. Biophys. Acta 1837 (2014) 1165–1177, http://dx.doi.org/10.1016/j.bbabio.2014.01.002.
[4] H.J. Lee, J. Reimann, Y. Huang, P. Adelroth, Functional proton transfer pathways in the heme-copper oxidase superfamily, Biochim. Biophys. Acta 1817 (2012) 537–544, http://dx.doi.org/10.1016/j.bbabio.2011.10.007.
[5] G. Brändén, R.B. Gennis, P. Brzezinski, Transmembrane proton translocation by cytochrome c oxidase, Biochim. Biophys. Acta Bioenerg. 1757 (2006) 1052–1063, http://dx.doi.org/10.1016/j.bbabio.2006.05.020.
[6] A.V. Pisliakov, P.K. Sharma, Z.T. Chu, M. Haranczyk, A. Warshel, Electrostatic basis for the unidirectionality of the primary proton transfer in cytochrome c oxidase, Proc. Natl. Acad. Sci. U. S. A. 105 (2008) 7726–7731, http://dx.doi.org/10.1073/pnas.0800580105.
[7] P. Goyal, J. Lu, S. Yang, M.R. Gunner, Q. Cui, Changing hydration level in an internal cavity modulates the proton affinity of a key glutamate in cytochrome c oxidase, Proc. Natl. Acad. Sci. U. S. A. 110 (2013) 18886–18891, http://dx.doi.org/10.1073/pnas.1313908110.
[8] V.R.I. Kaila, V. Sharma, M. Wikström, The identity of the transient proton loading site of the proton-pumping mechanism of cytochrome c oxidase, Biochim. Biophys. Acta 1807 (2011) 80–84, http://dx.doi.org/10.1016/j.bbabio.2010.08.014.
[9] I. Belevich, D.A. Bloch, N. Belevich, M. Wikström, M.I. Verkhovsky, Exploring the proton pump mechanism of cytochrome c oxidase in real time, Proc. Natl. Acad. Sci. U. S. A. 104 (2007) 2685–2690, http://dx.doi.org/10.1073/pnas.0608794104.
[10] R. Sugitani, E.S. Medvedev, A.A. Stuchebrukhov, Theoretical and computational analysis of the membrane potential generated by cytochrome c oxidase upon single electron injection into the enzyme, Biochim. Biophys. Acta 1777 (2008) 1129–1139, http://dx.doi.org/10.1016/j.bbabio.2008.05.006.
[11] J. Quenneville, D.M. Popović, A.A. Stuchebrukhov, Redox-dependent pK_a of Cu_B histidine ligand in cytochrome c oxidase, J. Phys. Chem. B 108 (2004) 18383–18389, http://dx.doi.org/10.1021/jp0467797.
[12] D.M. Popović, J. Quenneville, A.A. Stuchebrukhov, DFT/electrostatic calculations of pKa values in cytochrome c oxidase, J. Phys. Chem. B 109 (2005) 3616–3626, http://dx.doi.org/10.1021/jp046535m.
[13] J. Quenneville, D.M. Popović, A.A. Stuchebrukhov, Combined DFT and electrostatics study of the proton pumping mechanism in cytochrome c oxidase, Biochim. Biophys. Acta 1757 (2006) 1035–1046, http://dx.doi.org/10.1016/j.bbabio.2005.12.003.
[14] D.V. Makhov, D.M. Popović, A.A. Stuchebrukhov, Improved density functional theory/electrostatic calculation of the His291 protonation state in cytochrome c oxidase: self-consistent charges for solvation energy calculation, J. Phys. Chem. B 110 (2006) 12162–12166, http://dx.doi.org/10.1021/jp0608630.
[15] S. Supekar, A.P. Gamiz-Hernandez, V.R.I. Kaila, A protonated water cluster as a transient proton-loading site in cytochrome c oxidase, Angew. Chem. Int. Ed. Eng. 55 (2016) 11940–11944, http://dx.doi.org/10.1002/anie.201603606.
[16] J. Lu, M.R. Gunner, Characterizing the proton loading site in cytochrome c oxidase, Proc. Natl. Acad. Sci. U. S. A. 111 (2014) 12414–12419, http://dx.doi.org/10.1073/pnas.1407187111.
[17] D.M. Popović, A.A. Stuchebrukhov, Proton exit channels in bovine cytochrome c oxidase, J. Phys. Chem. B 109 (2005) 1999–2006, http://dx.doi.org/10.1021/jp0464371.
[18] S. Yoshikawa, K. Shinzawa-Itoh, R. Nakashima, R. Yaono, E. Yamashita, N. Inoue, M. Yao, M.J. Fei, C.P. Libeu, T. Mizushima, H. Yamaguchi, T. Tomizaki, T. Tsukihara, Redox-coupled crystal structural changes in bovine heart cytochrome c oxidase, Science 280 (1998) 1723–1729.
[19] T. Tsukihara, H. Aoyama, E. Yamashita, T. Tomizaki, H. Yamaguchi, K. Shinzawa-Itoh, R. Nakashima, R. Yaono, S. Yoshikawa, The whole structure of the 13-subunit oxidized cytochrome c oxidase at 2.8 A, Science 272 (1996) 1136–1144.
[20] S. Yoshikawa, A. Shimada, Reaction mechanism of cytochrome c oxidase, Chem. Rev. 115 (2015) 1936–1989, http://dx.doi.org/10.1021/cr500266a.
[21] H.M. Lee, T.K. Das, D.L. Rousseau, D. Mills, S. Ferguson-Miller, R.B. Gennis, Mutations in the putative H-channel in the cytochrome c oxidase from *Rhodobacter sphaeroides* show that this channel is not important for proton conduction but reveal modulation of the properties of heme a, Biochemistry 39 (2000) 2989–2996.
[22] V. Sharma, P.G. Jambrina, M. Kaukonen, E. Rosta, P.R. Rich, Insights into functions

of the H channel of cytochrome c oxidase from atomistic molecular dynamics simulations, Proc. Natl. Acad. Sci. U. S. A. 114 (2017) E10339–E10348, http://dx.doi.org/10.1073/pnas.1708628114.
[23] R. Sugitani, A.A. Stuchebrukhov, Molecular dynamics simulation of water in cytochrome c oxidase reveals two water exit pathways and the mechanism of transport, Biochim. Biophys. Acta Bioenerg. 1787 (2009) 1140–1150, http://dx.doi.org/10.1016/j.bbabio.2009.04.004.
[24] P. Goyal, S. Yang, Q. Cui, Microscopic basis for kinetic gating in cytochrome c oxidase: insights from QM/MM analysis, Chem. Sci. 6 (2014) 826–841, http://dx.doi.org/10.1039/C4SC01674B.
[25] A.-L. Johansson, M. Högbom, J. Carlsson, R.B. Gennis, P. Brzezinski, Role of aspartate 132 at the orifice of a proton pathway in cytochrome c oxidase, Proc. Natl. Acad. Sci. U. S. A. 110 (2013) 8912–8917, http://dx.doi.org/10.1073/pnas.1303954110.
[26] I.A. Smirnova, P. Adelroth, R.B. Gennis, P. Brzezinski, Aspartate-132 in cytochrome c oxidase from *Rhodobacter sphaeroides* is involved in a two-step proton transfer during oxo-ferryl formation, Biochemistry 38 (1999) 6826–6833, http://dx.doi.org/10.1021/bi982865j.
[27] G. Brändén, A.S. Pawate, R.B. Gennis, P. Brzezinski, Controlled uncoupling and recoupling of proton pumping in cytochrome c oxidase, Proc. Natl. Acad. Sci. U. S. A. 103 (2006) 317–322, http://dx.doi.org/10.1073/pnas.0507734103.
[28] D.M. Mitchell, J.R. Fetter, D.A. Mills, P. Adelroth, M.A. Pressler, Y. Kim, R. Aasa, P. Brzezinski, B.G. Malmström, J.O. Alben, G.T. Babcock, S. Ferguson-Miller, R.B. Gennis, Site-directed mutagenesis of residues lining a putative proton transfer pathway in cytochrome c oxidase from *Rhodobacter sphaeroides*, Biochemistry 35 (1996) 13089–13093, http://dx.doi.org/10.1021/bi961416l.
[29] L. Varanasi, J. Hosler, Alternative initial proton acceptors for the D pathway of *Rhodobacter sphaeroides* cytochrome c oxidase, Biochemistry 50 (2011) 2820–2828, http://dx.doi.org/10.1021/bi102002v.
[30] H. Mohrmann, J. Dragelj, F. Baserga, E.-W. Knapp, S.T. Stripp, J. Heberle, The reductive phase of *Rhodobacter sphaeroides* cytochrome c oxidase disentangled by CO ligation, Phys. Chem. Chem. Phys. (2017), http://dx.doi.org/10.1039/c7cp06480b.
[31] M. Sezer, A.-L. Woelke, E.W. Knapp, R. Schlesinger, M.A. Mroginski, I.M. Weidinger, Redox induced protonation of heme propionates in cytochrome c oxidase: insights from surface enhanced resonance Raman spectroscopy and QM/MM calculations, Biochim. Biophys. Acta 1858 (2017) 103–108, http://dx.doi.org/10.1016/j.bbabio.2016.10.009.
[32] A. Puustinen, M. Wikström, Proton exit from the heme–copper oxidase of Escherichia coli, Proc. Natl. Acad. Sci. U. S. A. 96 (1999) 35–37, http://dx.doi.org/10.1073/pnas.96.1.35.
[33] V.R.I. Kaila, M.I. Verkhovsky, G. Hummer, M. Wikström, Mechanism and energetics by which glutamic acid 242 prevents leaks in cytochrome c oxidase, Biochim. Biophys. Acta 1787 (2009) 1205–1214, http://dx.doi.org/10.1016/j.bbabio.2009.04.008.
[34] N. Ghosh, X. Prat-Resina, M.R. Gunner, Q. Cui, Microscopic pKa analysis of Glu286 in cytochrome c oxidase (*Rhodobacter sphaeroides*): toward a calibrated molecular model, Biochemistry 48 (2009) 2468–2485, http://dx.doi.org/10.1021/bi8021284.
[35] V.R.I. Kaila, M.I. Verkhovsky, G. Hummer, M. Wikström, Glutamic acid 242 is a valve in the proton pump of cytochrome c oxidase, Proc. Natl. Acad. Sci. U. S. A. 105 (2008) 6255–6259, http://dx.doi.org/10.1073/pnas.0800770105.
[36] M. Tsubaki, H. Hori, T. Mogi, Glutamate-286 mutants of cytochrome bo-type ubiquinol oxidase from Escherichia coli: influence of mutations on the binuclear center structure revealed by FT-IR and EPR spectroscopies, FEBS Lett. 416 (1997) 247–250.
[37] A.L. Woelke, G. Galstyan, A. Galstyan, T. Meyer, J. Heberle, E.-W. Knapp, Exploring the possible role of Glu286 in CcO by electrostatic energy computations combined with molecular dynamics, J. Phys. Chem. B 117 (2013) 12432–12441, http://dx.doi.org/10.1021/jp407250d.
[38] A.-L. Johansson, S. Chakrabarty, C.L. Berthold, M. Högbom, A. Warshel, P. Brzezinski, Proton-transport mechanisms in cytochrome c oxidase revealed by studies of kinetic isotope effects, Biochim. Biophys. Acta 1807 (2011) 1083–1094, http://dx.doi.org/10.1016/j.bbabio.2011.03.012.
[39] M. Svensson-Ek, J. Abramson, G. Larsson, S. Törnroth, P. Brzezinski, S. Iwata, The X-ray crystal structures of wild-type and EQ(I-286) mutant cytochrome c oxidases from *Rhodobacter sphaeroides*, J. Mol. Biol. 321 (2002) 329–339.
[40] J.E. Morgan, M.I. Verkhovsky, G. Palmer, M. Wikström, Role of the PR intermediate in the reaction of cytochrome c oxidase with O_2, Biochemistry 40 (2001) 6882–6892.
[41] Y. Song, J. Mao, M.R. Gunner, Calculation of proton transfers in bacteriorhodopsin bR and M intermediates, Biochemistry 42 (2003) 9875–9888, http://dx.doi.org/10.1021/bi034482d.
[42] Y. Song, E. Michonova-Alexova, M.R. Gunner, Calculated proton uptake on anaerobic reduction of cytochrome C oxidase: is the reaction electroneutral? Biochemistry 45 (2006) 7959–7975, http://dx.doi.org/10.1021/bi052183d.
[43] P. Shannon, A. Markiel, O. Ozier, N.S. Baliga, J.T. Wang, D. Ramage, N. Amin, B. Schwikowski, T. Ideker, Cytoscape: a software environment for integrated models of biomolecular interaction networks, Genome Res. 13 (2003) 2498–2504, http://dx.doi.org/10.1101/gr.1239303.
[44] M.R. Gunner, M. Amin, X. Zhu, J. Lu, Molecular mechanisms for generating transmembrane proton gradients, Biochim. Biophys. Acta Bioenerg. 1827 (2013) 892–913, http://dx.doi.org/10.1016/j.bbabio.2013.03.001.
[45] C. Hiser, L. Buhrow, J. Liu, L. Kuhn, S. Ferguson-Miller, A conserved amphipathic ligand binding region influences k-path-dependent activity of cytochrome C oxidase, Biochemistry 52 (2013) 1385–1396, http://dx.doi.org/10.1021/bi3014505.
[46] J. Liu, C. Hiser, S. Ferguson-Miller, Role of conformational change and K-path ligands in controlling cytochromecoxidase activity, Biochem. Soc. Trans. 45 (2017) 1087–1095, http://dx.doi.org/10.1042/BST20160138.
[47] T. Ghane, R.F. Gorriz, S. Wrzalek, S. Volkenandt, F. Dalatieh, M. Reidelbach, P. Imhof, Hydrogen-bonded network and water dynamics in the D-channel of cytochrome c oxidase, J. Membr. Biol. (2018), http://dx.doi.org/10.1007/s00232-018-0019-x.
[48] P.E.M. Siegbahn, M.R.A. Blomberg, Mutations in the D-channel of cytochrome c oxidase causes leakage of the proton pump, FEBS Lett. 588 (2014) 545–548, http://dx.doi.org/10.1016/j.febslet.2013.12.020.
[49] G. Gilderson, L. Salomonsson, A. Aagaard, J. Gray, P. Brzezinski, J. Hosler, Subunit III of cytochrome c oxidase of *Rhodobacter sphaeroides* is required to maintain rapid proton uptake through the D pathway at physiologic pH, Biochemistry 42 (2003) 7400–7409, http://dx.doi.org/10.1021/bi0341298.
[50] S. Yoshikawa, K. Muramoto, K. Shinzawa-Itoh, H. Aoyama, T. Tsukihara, K. Shimokata, Y. Katayama, H. Shimada, Proton pumping mechanism of bovine heart cytochrome c oxidase, Biochim. Biophys. Acta Bioenerg. 1757 (2006) 1110–1116, http://dx.doi.org/10.1016/j.bbabio.2006.06.004.
[51] R. Liang, J.M.J. Swanson, Y. Peng, M. Wikström, G.A. Voth, Multiscale simulations reveal key features of the proton-pumping mechanism in cytochrome c oxidase, Proc. Natl. Acad. Sci. U. S. A. 113 (2016) 7420–7425, http://dx.doi.org/10.1073/pnas.1601982113.
[52] S.A. Seibold, D.A. Mills, S. Ferguson-Miller, R.I. Cukier, Water chain formation and possible proton pumping routes in *Rhodobacter sphaeroides* cytochrome c oxidase: a molecular dynamics comparison of the wild type and R481K mutant, Biochemistry 44 (2005) 10475–10485, http://dx.doi.org/10.1021/bi0502902.
[53] C.Y. Son, A. Yethiraj, Q. Cui, Cavity hydration dynamics in cytochrome c oxidase and functional implications, Proc. Natl. Acad. Sci. U. S. A. 114 (2017) E8830–E8836, http://dx.doi.org/10.1073/pnas.1707922114.
[54] P. Brzezinski, R.B. Gennis, Cytochrome c oxidase: exciting progress and remaining mysteries, J. Bioenerg. Biomembr. 40 (2008) 521–531, http://dx.doi.org/10.1007/s10863-008-9181-7.
[55] R. Schneider, A. de Daruvar, C. Sander, The HSSP database of protein structure-sequence alignments, Nucleic Acids Res. 25 (1997) 226–230.
[56] M. Wikström, M.I. Verkhovsky, G. Hummer, Water-gated mechanism of proton translocation by cytochrome c oxidase, Biochim. Biophys. Acta 1604 (2003) 61–65.
[57] D.A. Mills, S. Ferguson-Miller, Influence of structure, pH and membrane potential on proton movement in cytochrome oxidase, Biochim. Biophys. Acta 1555 (2002) 96–100.
[58] P.R. Magalhães, A.S.F. Oliveira, S.R.R. Campos, C.M. Soares, A.M. Baptista, Effect of a pH gradient on the protonation states of cytochrome c oxidase: a continuum electrostatics study, J. Chem. Inf. Model. 57 (2017) 256–266, http://dx.doi.org/10.1021/acs.jcim.6b00575.
[59] L.S. Busenlehner, G. Brändén, I. Namslauer, P. Brzezinski, R.N. Armstrong, Structural elements involved in proton translocation by cytochrome c oxidase as revealed by backbone amide hydrogen-deuterium exchange of the E286H mutant, Biochemistry 47 (2008) 73–83, http://dx.doi.org/10.1021/bi701643a.
[60] B. Schmidt, J. McCracken, S. Ferguson-Miller, A discrete water exit pathway in the membrane protein cytochrome c oxidase, Proc. Natl. Acad. Sci. U. S. A. 100 (2003) 15539–15542, http://dx.doi.org/10.1073/pnas.2633243100.
[61] K. Ganesan, R.B. Gennis, Blocking the K-pathway still allows rapid one-electron reduction of the binuclear center during the anaerobic reduction of the aa3-type cytochrome c oxidase from *Rhodobacter sphaeroides*, Biochim. Biophys. Acta 1797 (2010) 619–624, http://dx.doi.org/10.1016/j.bbabio.2010.03.012.
[62] S. Jünemann, B. Meunier, R.B. Gennis, P.R. Rich, Effects of mutation of the conserved lysine-362 in cytochrome c oxidase from *Rhodobacter sphaeroides*, Biochemistry 36 (1997) 14456–14464, http://dx.doi.org/10.1021/bi971458p.
[63] A.S. Pawate, J. Morgan, A. Namslauer, D. Mills, P. Brzezinski, S. Ferguson-Miller, R.B. Gennis, A mutation in subunit I of cytochrome oxidase from *Rhodobacter sphaeroides* results in an increase in steady-state activity but completely eliminates proton pumping, Biochemistry 41 (2002) 13417–13423.
[64] T.V. Vygodina, C. Pecoraro, D. Mitchell, R. Gennis, A.A. Konstantinov, Mechanism of inhibition of electron transfer by amino acid replacement K362M in a proton channel of *Rhodobacter sphaeroides* cytochrome c oxidase, Biochemistry 37 (1998) 3053–3061, http://dx.doi.org/10.1021/bi971876u.
[65] D.A. Mills, L. Florens, C. Hiser, J. Qian, S. Ferguson-Miller, Where is “outside” in cytochrome c oxidase and how and when do protons get there? Biochim. Biophys. Acta 1458 (2000) 180–187.
[66] J. Qian, D.A. Mills, L. Geren, K. Wang, C.W. Hoganson, B. Schmidt, C. Hiser, G.T. Babcock, B. Durham, F. Millett, S. Ferguson-Miller, Role of the conserved arginine pair in proton and electron transfer in cytochrome C oxidase, Biochemistry 43 (2004) 5748–5756, http://dx.doi.org/10.1021/bi036279o.
[67] D.A. Mills, L. Geren, C. Hiser, B. Schmidt, B. Durham, F. Millett, S. Ferguson-Miller, An arginine to lysine mutation in the vicinity of the heme propionates affects the redox potentials of the hemes and associated electron and proton transfer in cytochrome c oxidase, Biochemistry 44 (2005) 10457–10465, http://dx.doi.org/10.1021/bi050283d.